Pore translocation of knotted DNA rings

Antonio Suma[a] **and Cristian Micheletti**[a]

[a]SISSA, International School for Advanced Studies, via Bonomea 265, I-34136 Trieste, Italy

This manuscript was compiled on April 28, 2022

We use an accurate coarse-grained model for DNA, oxDNA, and stochastic molecular dynamics simulations to study the pore translocation of 10Kbp-long DNA rings that are knotted. By monitoring various topological and physical observables we find that there is not one, as previously assumed, but rather two qualitatively different modes of knot translocation. For both modes the pore obstruction caused by knot passage has a brief duration and typically occurs at a late translocation stage. Both effects are well in agreement with experiments, and can be rationalised with a transparent model based on the concurrent tensioning and sliding of the translocating knotted chains. We also observed that the duration of the pore obstruction event is more controlled by the knot translocation velocity than the knot size. These features ought to advance the interpretion and design of future experiments aimed at probing the spontaneous knotting of biopolymers.

DNA knotting | Pore translocation | Molecular dynamics simulations

How filamentous molecules behave when driven through a narrow pore is one of the classic, yet still open questions in polymer physics. The problem has important applications for single-molecule manipulation techniques, including the sequencing of single-stranded DNA filaments (1–8), and is relevant for fundamental research as well, particularly for biological systems where the processing of DNA (9, 10), RNA (11) and protein chains (12) often depends on their active translocation through narrow pores.

Because knots are statistically inevitable in long polymers and biopolymers (13–20), a relevant question is how such forms of entanglement affect pore translocation (21–34).

Very recently, an important advancement in this research field has been made by Plesa *et al.* (34) who succeeded in devising an advanced single-molecule experiment where double-stranded DNA was translocated through a solid-state nanopore in carefully controlled conditions. The DNA filaments were sufficiently long to be spontaneously knotted in a sizeable fraction of the equilibrium population. The pore diameter, 10-20nm, was purposely chose to be smaller than the DNA persistence length, $l_p = 50$nm, and yet wide enough to accommodate several dsDNA strands, and hence let knots through. A surprisingly rich phenomenology was found for the main monitored observables. These were the elapsed time at which the pore was obstructed by the passing knot, and the duration of the obstruction event. The latter had a rapidly decaying distribution, and an elegant, indirect interpretation was offered in terms of the self-tightened knots predicted in refs. (35). The distribution of the timing of the obstruction events remained, however, elusive to explain.

Here, to advance the understanding of the process and its relationship with DNA knotting in equilibrium, we present a detailed study based on molecular dynamics simulations of an accurate mesoscopic DNA model. Specifically, we consider equilibrated knotted DNA rings of 10K base-pairs (bp) in the oxDNA (36–39) representation and use Langevin dynamics to simulate their driven passage through a 10nm-wide pore. Such theoretical and computational framework allows us to investigate the translocation process and the geometry-topology interplay with unprecedented structural and dynamical detail.

Our main findings are the following. First, we observe that there is another mode of knot translocation besides the one that has been considered so far. Secondly, the passage of the entangled region through the pore is largely controlled by the positioning of the knot on the ring, and its velocity at the time of translocation. As a consequence, pore obstruction events associated to knot passage are brief and mostly occur at late translocation stages. Finally, these properties, which are in good overall accord with single-molecules experiments, are recapitulated with a schematic interpretative model which can also be used for predictive purposes.

Results and discussion

System setup. We carried out various Langevin dynamics simulations of knotted DNA rings translocating through a nanopore embedded in a slab, see Fig. 1. The rings, modelled mesoscopically with oxDNA (36–39), were 10Kbp long and were nicked, to allow relaxation of torsional stress, as in typical experiments (34, 40). The translocation is driven by a longitudinal electric field exerting a force of 0.2pN on each nucleotide inside the pore. For simplicity, we neglect the action of the field outside the pore (41, 42) that, in actual realizations, can facilitate the capture and pore insertion of the knotted chains (43–45). The pore is 10nm wide and 10nm long, so that each of the two dsDNA filaments inside it ($\sim$ 30bp-long) is pulled with a total force of 12pN.

The translocation dynamics was studied for 50 different equilibrated knotted DNA configurations. These were gener-

Significance Statement

Pore translocation, the driven passage of molecules through narrow channels, has become an important tool for probing DNA properties. In a recent breakthrough experiment, this technique was used to detect knots that form spontaneously in DNA filaments and can hence impact the *in vivo* functionality. Here, by using an accurate model, we simulate the translocation of knotted DNA, expose its unexpectedly rich phenomenology and clarify the implications for experiments. We show that knot translocation occurs in two possible modes, depending on the knot initial position and size. These properties also account for the typically late occurrence of the knot passage event. Finally, the passage duration is found to depend more on the translocation velocity of the knot than its size.

Reserved for publication notes

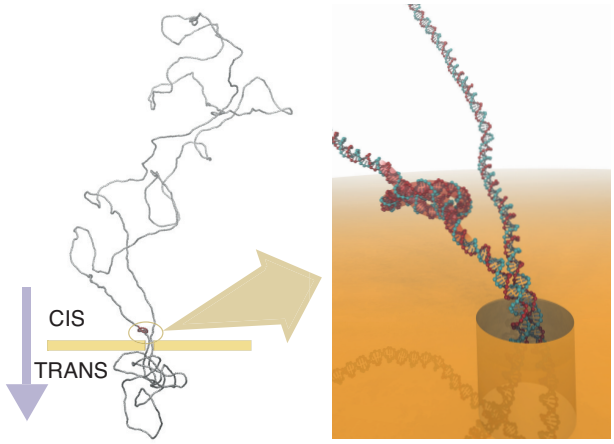

Fig. 1. Typical configuration of a knotted double-stranded DNA ring translocating through a nanopore. The knot approaching the pore entrance is highlighted in the inset. The ring, which is modelled with oxDNA, is 10Kbp-long and the pore, which is 10nm wide, is embedded in an impenetrable 10nm-thick slab. A translocating force of 0.2pN is applied to each nucleotide inside the pore.

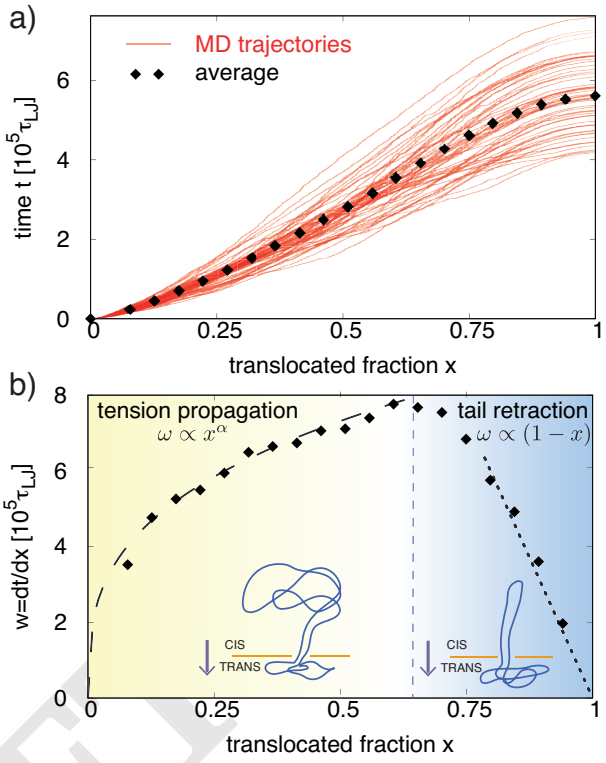

Fig. 2. a) The time required to translocate a fraction x of the knotted DNA rings is shown for 50 independent simulations (red curves). The black points show the average $\langle t \rangle$ versus x curve. b) The waiting time curve, $w = \frac{d\langle t \rangle}{dx}$ highlights two main regimes corresponding to the tension propagation along the chain ($x \lesssim 0.5$) followed by the translocation of the rectified chain tail ($x \gtrsim 0.75$). The dashed and dotted lines are best fits based, respectively, on $w \propto x^{\alpha}$ (yielding $\alpha \sim 0.32$) and $w \propto (1-x)$.

ated with a Monte Carlo scheme applied to a coarse-grained DNA model and were subsequently refined and relaxed with the oxDNA model. All configurations featured a trefoil or 3_1 knot, which is by far the dominant topology at the considered DNA length (17, 32, 46). These initial configurations were primed at the pore entrance at a random point lying on their convex hull.

Translocation dynamics overview. For a first, general characterization of the process we profiled the translocated fraction of the chain, x, as a function of the elapsed simulation time, t. This dependence is shown in Fig.2a where, as customary, it is presented as a t versus x plot. The red curves cover the individual trajectories while the filled points represent the average curve.

Fig.2b shows, instead, the so-called waiting time (47), $w = dt/dx$, i.e. the inverse of the translocation velocity, whose profile clearly outlines the two known main translocation regimes (45, 47, 48).

The first part of the curve, for $x \lesssim 0.5$, corresponds to the tension propagation along the chain, which itself presents an articulate phenomenology (49–51). For chains that are asymptotically long and free of entanglement, theoretical scaling arguments predict a power-law behaviour, $w \propto x^{\nu}$, where $\nu = 0.586$ is the metric exponent for self-avoiding walks (47, 49, 52–55), while smaller effective exponents are expected for chains of finite length (47, 56). Fig. 2b shows that data points for the 10Kbp chains are indeed well fitted by a power law, and the effective exponent, 0.32, is close to what previously reported at comparable DNA lengths (57).

At $x \sim 0.6$ the tension propagation regime crosses over to the tail retraction regime. In this stage the still untranslocated remainder of the chain, which is fully rectified, accelerates towards the pore. Because the pore is large enough to let the whole knot pass through, this second stage too follows the behaviour expected theoretically, $w \propto (1-x)$ (47).

Statistics of knot translocation events. Inspired by experiments, we detect the passage of the knot through the pore by monitoring the degree of obstruction of the latter. During such event, in fact, the pore lumen must accommodate up to four double-stranded filaments, instead of the usual two, see sketches in Fig. 3a.

We accordingly monitored the time evolution of the chain fraction inside the pore, Δx, which is shown in Fig. 3a. The pore obstruction caused by the passing knot is indeed signalled by a bump that stands out against the Δx baseline, see Fig. 3b. Notice that this major pore obstruction event is preceded by a smaller signal burst caused by the knot partially entering the pore and then retracting from it. Such translocation attempts, illustrated in Movies S1-S2, affect about 50% of the trajectories. Their occurrence arguably depends on frictional effects arising from the geometry of the knot and the direction with which it engages the pore.

Various observables of interest, related to those monitored in the experiments of ref. (34), can be derived from the analysis of the Δx profile: the fraction of the translocated chain at which the pore-obstruction event takes place, x^*, the elapsed time at which it occurs, t^*, and the temporal duration of the event, Δt^*. Because t^* and x^* are monotonically related, we will focus on x^* and Δt^*, whose probability distributions are shown in Fig. 3c-d.

The key features are two. First, the distribution of x^* is skewed towards large values of x^*, see Fig. S1 for the same effect in the companion distribution of t^*. In fact, passage

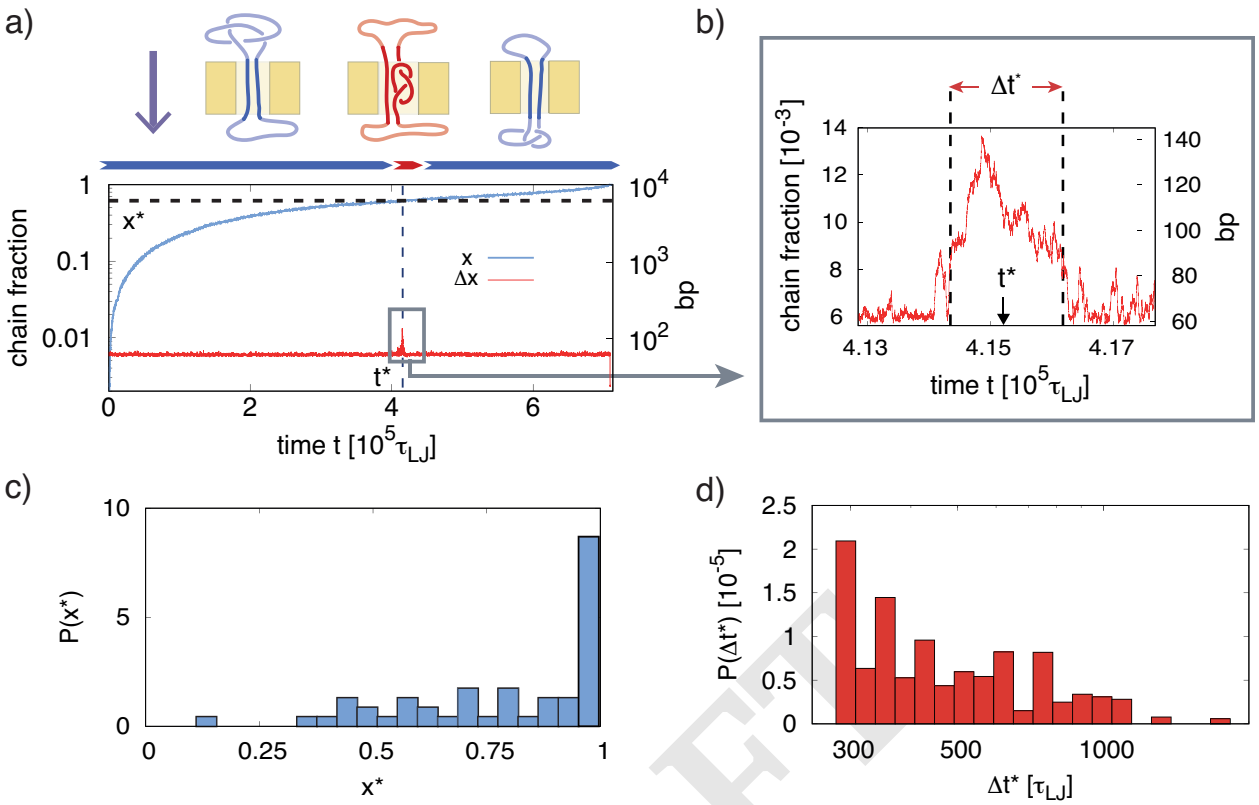

Fig. 3. a) Time evolution of the chain fraction that is inside the pore, Δx (red), and that has already translocated through it, x (blue). An absolute scale in base-pairs for x and Δx is also provided for the semi-log plot. The knot passage event is highlighted in panel b) and its time of occurrence, t^*, is defined as the midpoint of the time interval Δt^* during which Δx exceeds by more than 30% its baseline value. Panels c) and d) show the probability distributions, computed over the 50 independent runs, of the translocated chain fraction at the passage (pore obstruction) event, x^*, and of the event duration, Δt^*, respectively.

events are virtually absent for $x^* < 0.3$ and the distribution is prominently peaked at $x^* \sim 1$. Secondly, the distribution of the obstruction duration has an overall decreasing trend, with the shortest obstruction events (which have a minimum duration of 300 τ_{LJ}) being the most probable too. Both these features match the ones reported by Plesa *et al.*.

This consistency of the experimental and theoretical distributions for x^* and Δt^* is noteworthy given the different contour lengths considered here (10Kbp) and in the experiment (20Kbp or longer). This underscores the robustness of the effects addressed with either of the two approaches. The agreement also gives confidence for using the model to gain insight into aspects that cannot be directly accessed with current experiments. These primarily include various properties of the knotted region, which we discuss in the following.

Knot translocation modes. As we discuss, both the position of the knot along the chain contour and its size affect the Δt^* and x^* distributions in ways that are much richer than previously suspected.

A particularly intriguing relationship is found between the pore obstruction duration, Δt^*, and the size of the knotted region, l_k, when it arrives at the pore. We recall that, as customary, the knotted portion is identified as the shortest portion of the chain that, upon closure, has the same topology of the entire ring. A scatter plot of the two quantities is presented in Fig. 4a, where two relevant features are noted. First, the datapoints occupy an L-shaped region. Secondly, for either arm of this region the correlation between Δt^* and l_k is rather weak. Both aspects are not intuitive and, in fact, had not been previously predicted nor envisaged.

The analysis of the trajectories showed that the distinct arms in the diagram of Fig. 4a originate from two different modes of knot translocation, as described below.

In the first mode the knot is tight and localised on one of the two translocating filaments, see Fig. 4d. This is the most intuitive type of knot passage and, in fact, it was the mode of choice used in ref. (34) to interpret the experimental data on Δt^* and thus obtain a mapping between pore-obstruction time and knot length. By using a linear mapping, Plesa *et al.* were able to conclude that knots could be rather tight upon translocation, spanning an arclength of tens of nanometers, hence comparable to the DNA persistence length. This result was further put in the context of the elegant theory of metastable knots, which predicts knot localization based on the fact that, in the otherwise broad distribution of knot lengths, the most probable one is about constant - rather than growing - with chain length.

Our results vividly confirm the significant occurrence of tight knots. Indeed, one observes that the average knot length at the passage event is about 54nm, which is in full accord with the estimate of Plesa *et al.*. This knot length is reached independently of the initial one thanks to tightening of the knot caused by the propagating chain tension, see Fig. 4b. One also notes that the l_k versus Δt^* profile in Fig. 4a is rather

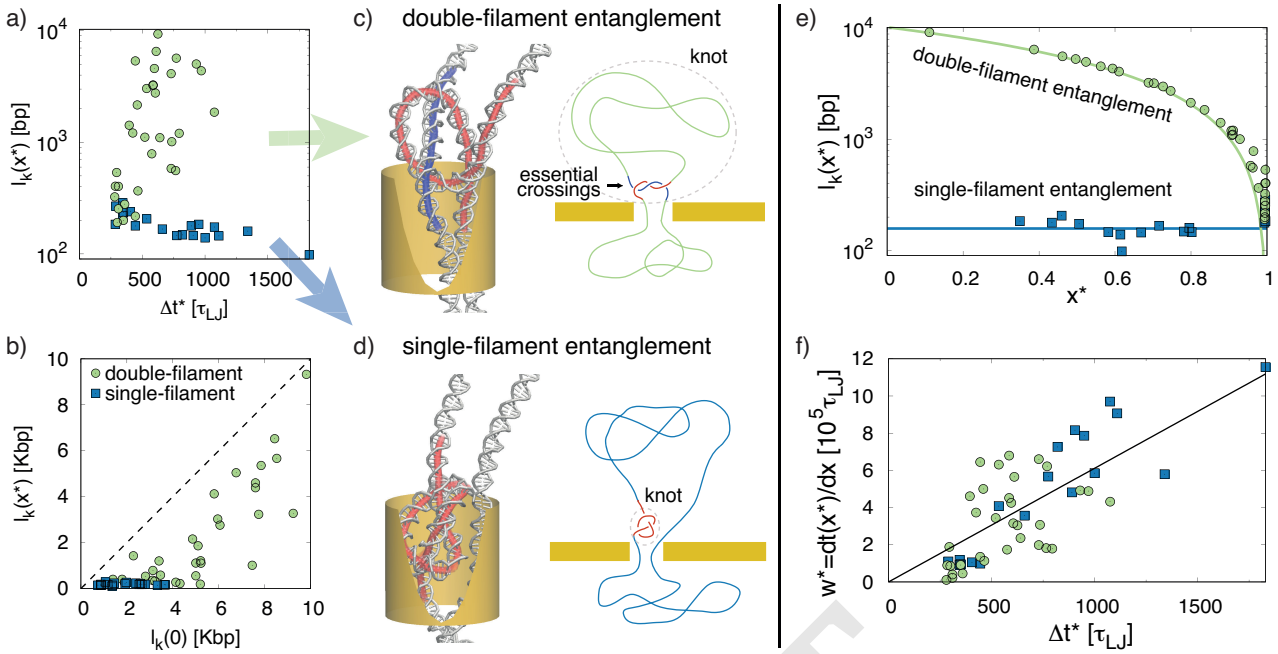

Fig. 4. a) Scatter plot of the knot length at the pore obstruction event, $l_k(x^*)$, versus the duration of the event itself, Δt^*. b) Knot length at the beginning of the translocation process, $l_k(0)$, and at the pore obstruction event, $l_k(x^*)$. Data points are divided in two classes based on whether the knot at the *beginning* of the translocation straddled (green) or not straddled (blue) the site antipodal (on the ring contour) to the translocation initiation site, see main text. For the first group, the pore obstruction event practically involves only the essential crossings of the knotted region, which spans both translocating filaments, see panel c. For the second group, the pore obstruction is caused by a single-filament knot, see panel d. e) Knot length l_k during pore obstruction at x^*. Data points for double-filament knots follow closely the curve $l_k = l_{chain}(1 - x^*)$ (solid green line), while for the other points l_k is about constant and equal to 160bp. f) Scatter plot of Δt^* against the waiting time w^* at the time of passage.

flat for this translocation mode, and hence is different from the linear relationship expected intuitively. An explanation of this effect will be discussed later.

The second, and new mode is associated to the green points in Fig. 4. It involves knots that span a significant portion of the ring, consistent with the theoretical results of ref. (58) on DNA chains of comparable size, which indicated that the most probable knot length is about 2200bp. In fact, these knots experience significantly less tightening during translocation than those discussed above, see Fig. 4b. Intriguingly, these knots are large and yet their pore-obstruction times are not at all dissimilar from the tight knot case discussed before.

This conundrum is solved by considering the actual conformation of such rings when the knot is presented at the pore entrance. A typical configuration is shown in Fig. 4c. The accompanying sketch clarifies that the knotted portion now spans the entire *cis* part of the ring. This is quantitatively shown in the semi-log plot of Fig. 4e where one observes that for this class of knots, the relative chain fraction occupied by the knot is $l_k/l_{chain} \sim (1 - x^*)$.

However, a significant obstruction of the pore occurs only when the region accommodating the essential crossings passes through it. As seen in the figure, this region is typically small, involving 123bp (42nm) on average.

It is therefore this short, essentially-entangled portion of "double-filament" knots, and not their entire contour lengths, l_k, that is captured by Δt^*.

To our knowledge, the possible occurrence of a second mode of translocation, though rather natural *a posteriori*, has not been considered nor foreseen in previous translocation studies, neither for dsDNA rings experiments, nor for simulations of linear, open chains where it can also occur if translocation starts from inside the knot loop region.

Notice that, because the essentially-entangled region is comparable in size to the tight, single-filament knots, the two modes of translocation cannot be distinguished from the sole analysis of Δt^*. This has direct bearings on the interpretation of experimental data. In fact, it poses the necessity to devise suitable means of discriminating or controlling the incidence of the two modes. IN this way one could relate more reliably the measured observables to the spontaneous knotting properties of DNA. Our results suggest that this could be achieved, for instance, by suitably choosing the DNA length. The latter, in fact, affects the balance of the two modes, as we discuss later in connection with Fig. 5a.

We conclude the analysis of the data in Fig. 4a by discussing the second notable feature, namely the lack of a noticeable correlation between the pore obstruction duration, Δt^*, and knot length, l_k. For the second mode of translocation, it is now clear that no obvious relationship between l_k and Δt^* can be expected, because the l_k is not directly informative for the pore obstruction caused by the essentially-entangled region. The case is different, however, for the first mode, i.e. tight single-filament knots, where a proportionality relationship between knot size and passage time appears plausible and was previously surmised (34).

This point is clarified by the plot of Fig. 4f, which shows the relationship between Δt^* and w^*, the inverse translocation velocity at the passage event. The two quantities are visibly correlated for both knot translocation modes. Together with

the plot Fig. 4a the data clarify that of these two properties relatable the passage time, knot length and knot translocation velocity, the dominant one is the latter. Notice that, because at passage time the contour lengths of single-filament knots and of double-filament essential crossings spans a limited range, from 120bp to 160bp, one has that Δt^* and w^* have an approximate linear proportionality.

This observation might be harnessed to extract further knot-related properties from Δt^*. Because the average translocation velocity depends on the translocated chain fraction, the observed Δt^* vs w^* correlation should effectively subsume a dependence of Δt^* on the knot position along the chain contour, x^*, which could be recovered with sufficient statistics.

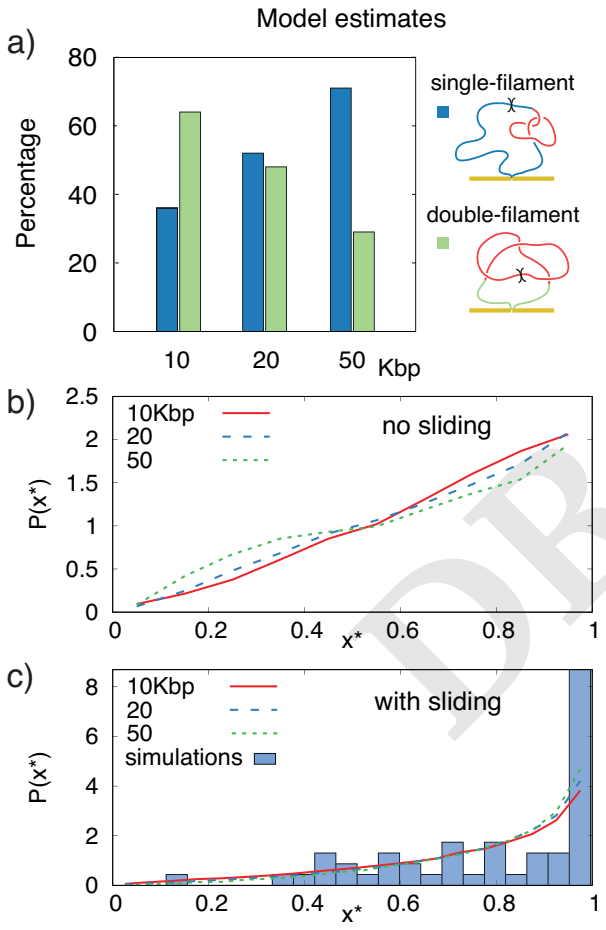

Fig. 5. a) Model estimate of relative percentage of single- and double-filament knots in DNA rings of different length. The estimate considers the length and positioning of the knotted region (highlighted in red in the sketches) with respect to the point (marked with a cross) antipodal to the root. b) The same model is used to predict the translocated chain fraction at the time of the pore obstruction event, x^*, see panel (b). Accounting for the sliding of the knot along the chain brings the model distribution in good quantitative agreement with the actual simulation data, see panel (c).

Interpretative model. We now consider the origin of the two different translocation modes and of the skewed distribution of the knot position at passage time, x^*.

Both aspects are best illustrated with the following schematic model of the translocation process. In this purposely simplified scheme we assume that the rooting point where the translocation process initiates is equally likely to lie anywhere on the ring contour. We also assume that tension propagates in the same way along the two ring arms, so that they meet at the antipodal midpoint, that is at the point at half ring contour length from the root.

The main discriminator for the two translocation modes is whether the knot is entirely located on only one of the two arms, or whether it straddles the antipodal midpoint and hence spans both arms, see sketches in Fig. 5.

In the former case the sliding of the progressively tensioned ring arm causes the knotted region to tighten towards the distal knot end (i.e. the end that is furthest from the rooting point) while it is dragged to the pore, see Movie S3. The tightened single-filament knot will then pass through the pore.

Instead, when the knotted region straddles the antipodal midpoint, the knot will be pulled from both sides and will be dragged towards the pore by both tensioned arms. Such double pulling typically causes the essential crossings to become interlocked, trapping the knot in a moderate degree of tightening, see Movie S4. The pore obstruction event is then associated to the passage of the essential crossings.

These two cases are directly associated to the two different translocation modes highlighted in Fig. 4. So much so that the two sets in the figure were not assigned from an *a posteriori* supervised inspection of the trajectories, but rather *a priori* based on the aforementioned distinction. In fact, the two sets precisely correspond to knots that span a single or both ring arms at the *beginning* of translocation. The neat separation of the two sets of points in Figs. 4a,b,e,f supports the viability and usefulness of such discriminatory criterion.

The same criterion can be also used to estimate how the relative incidence of single- versus double-filament entanglement varies with ring length. We considered an ensemble of Monte Carlo-generated rings of length 10, 20 and 50 Kbp, picked a rooting point randomly along their contour and then located the knot on the ring, which we considered open in correspondence of the rooting point. The rings were next assigned to one of the two classes based on whether the knotted region straddled the antipodal midpoint or not. The results, given in Fig. 5a, show that the incidence of single-filament entanglement increases steadily with chain length, and goes from 35% for 10Kbp to 70% for 50Kbp. Based on this result, which reflects the interplay of knot and chain lengths (35, 58–61), we speculate that most of the knot passage events detected in the experiment of Plesa *et al.* pertained to single-stranded entanglements, as implicitly assumed by the authors.

The same schematic framework can account for the qualitative features of the distribution of x^*, the knot positioning at time of translocation. We considered, again, the Monte Carlo generated ensemble of rings for which we stochastically-picked the rooting points. Next, for double-filament knots (straddling the antipodal midpoint) we picked x^* uniformly between the two knot ends. For the other, single-filament knots, we picked x^* as the distal end of the knot, the one further from the pore. These criteria embody in the simplest possible way the phenomenology described in the previous paragraphs.

The resulting probability distributions for x^*, shown in Fig. 5b, are in qualitative agreement with simulation and experimental data. It is seen that, at all ring lengths, the

distributions are skewed towards $x^* = 1$. As for the balance of single- and double-filament knots, the skewness too depends on the interplay of knot and ring length. Indeed, the x^* distribution becomes flatter for longer rings, where the knotted region occupies a smaller fraction of the chain contour.

The above modelling scheme neglects the possibility that tight knots may slide on the filament contour. As was clarified in the theoretical study of ref. (27, 30, 31), such sliding can occur for fully-flexible chains and, in fact, make it possible for individual knotted filaments to fully translocate through very narrow pores, as long as the driving force is not high enough to cause jamming (30, 62, 63). As a matter of fact, we observed the same knot sliding phenomenology for the present dsDNA system too, see Movie S1-S3.

To account for such sliding effect for single-filament knots, we accordingly adjusted the model. Specifically, we assumed that x^* could fall with equal probability between the distal knot end and the antipodal midpoint. The x^* probability distribution predicted by such model is shown in Fig. 5c. It presents a noticeably stronger shift forwards x^* values that follows closely the data from the simulated trajectories. This good level of agreement is somewhat surprising given the simplicity of the model, which does not account for frictional effects related to pore size and force magnitude. Yet, the good accord further corroborates the relevance of sliding effects for dsDNA. We believe, this would be an important avenue to explore further, especially by seeking a quantitative comparison against experimental data. For this, it would probably become essential to take into account the finite resolution of time measurements which could account for the observed effective dependence of the distribution of t^* (related monotonically, but non-linearly, to x^*) on the driving force.

Conclusions and perspectives

It is only very recently, that innovative single-molecule techniques have made it possible to detect knots in double-stranded DNA chains driven through nanopores (34). On the one hand, this gave a striking demonstration of spontaneous knot formation in linear and circularised DNA. On the other hand it also helped unveil a rich and complex phenomenology that, though expectedly relevant for the *in vivo* processing of DNA filaments, is still largely unexplored.

Here, to advance the understanding and characterization of such phenomenology, we studied theoretically the pore translocation of knotted DNA rings using an accurate coarse-grained model for DNA and stochastic molecular dynamics simulations.

We find good agreement with the experimental data, particularly regarding the remarkably brief duration of pore-obstruction events associated to the passage of the knot. By profiling the dynamical evolution of the knotted DNA rings we expose unexpectedly rich properties of the process that cannot be directly accessed in current experiments.

First, we found that translocation of the knotted region can occur in two qualitatively modes depending on whether the knot is dragged to the pore by only one of the ring arms, or both. In the latter case, knots are typically not tight, and yet we find that the pore obstruction time can be small (as in experiments) because the essential crossings of the knot coalesce in a short region.

Secondly, we found that the sliding and tensioning of the translocating knot causes the same bias towards late knot passage events found in experiments, and previously unexplained. We finally show that one of the key determinants of the pore obstruction duration is the initial positioning of the knot along the chain, and suggest how this effect might be deconvolved in experimental measurements for a more precise determination of the length of the region accommodating a knot or its essential crossings. In particular, the occurring phenomenon of knot sliding might give an important contribution. This might be exploitable in future experiments, along with chain length and pore size variations, to discriminate the two modes. Further relevant avenues include the impact on pore translocation of complex topologies such as composite knots, which have so far been characterised for flexible chains only (30), as well as the geometry-topology interplay in DNA rings that cannot relax supercoiling and torsional stress (64).

This first theoretical account, provides a detailed and physically-appealing insight into phenomenology of knotted dsDNA pore translocation. It provides a valuable and transparent interpretative framework for available experimental data while pointing out specific directions for new experiments as well as theoretical ones aimed at better understanding the implication of intra-chain entanglement for the *in vivo* processing of DNA, and possibly other biopolymers too.

Materials and Methods

System setup and simulation details For an accurate, mesoscopic description of double-stranded DNA we used oxDNA (36–39). In this model, nucleotides are treated as rigid and described by three-interaction centers. The potential energy includes terms that account for the chain connectivity, bending rigidity, base-pairing, screened electrostatic interactions and stacking effects. These terms are parametrised to reproduce the salient structural and equilibrium properties of nucleic acids filaments at various values of the system temperature and salt concentration, here set to $T = 300$K and 1M NaCl, respectively.

The initial conformations of the 10Kbp-long DNA rings were obtained by mapping the oxDNA model on top of knotted, coarsed DNA rings sampled with a topologically-unrestricted Monte Carlo scheme (46). These initial configurations, which model those obtained experimentally by circularization of linear DNA with so-called sticky-ends, were then nicked and primed at the entrance of the 10nm-wide pore, which was embedded in a 10nm thick impenetrable slab. The translocation process, simulated with Langevin dynamics using the oxDNA software package, was driven by applying a force of 0.2pN to each nucleotide inside the pore. Because the average number of nucleotides occupying the pore at any given time is 120, the average total driving force is 24pN (12pN on each of the two double-stranded filaments), which is about equal to what used in experiments. The constant-temperature ($T = 300$K) molecular dynamics was integrated, without hydrodynamic effects, with a time step of $0.005\tau_{LJ}$, where τ_{LJ} is the standard Lennard-Jones time unit for the simulations. Further details about the system setup are given in Fig. S2. An approximate mapping with real time can be obtained by matching the actual diffusion coefficient of small oxDNA fragments of 4bps with that expected in water for spheres with 1.27nm diameter, yielding $\tau_{LJ} \sim 0.7$ns. Based on this time mapping, the typical translocation time of Fig.2a is 400μs, which, for longer

chains of 50Kbp extrapolates to about 5ms, which compares well with experimental measurements available for this chain length (40).

Observables. The passage of a knot, or of its essential crossings, through pore was revealed by monitoring the number of nucleotides inside the pore and detecting increases by more than 30% from the baseline value, which is about equal to 60bp. This threshold criteria, which was validated by supervised visual inspection, was also used to establish the duration of the time interval associated to the passage of the knot through the pore.

For each instantaneous configuration, the location of the knot was identified with a bottom-up search. Specifically, we used the stochastic search scheme of ref. (65) to identify the shortest portion of the ring that, after suitable closure, has the same topology of the original ring. The search is limited to the *trans* or *cis* parts of the rings, respectively, depending on whether the knot has or has not already translocated through the pore.

ACKNOWLEDGMENTS. We thank Flavio Romano and Lorenzo Rovigatti for technical advice on the use of the oxDNA package. We acknowledge support from the Italian ministry of education, grant PRIN 2010HXAW77.

1. D Deamer, M Akeson, D Branton, Three decades of nanopore sequencing. *Nat. Biotechnol.* **34**, 518–524 (2016).
2. SJ Heerema, C Dekker, Graphene nanodevices for dna sequencing. *Nat. Nanotechnol.* **11**, 127–136 (2016).
3. S Agah, M Zheng, M Pasquali, AB Kolomeisky, Dna sequencing by nanopores: advances and challenges. *J.Phys.D* **49**, 413001 (2016).
4. Y Feng, Y Zhang, C Ying, D Wang, C Du, Nanopore-based fourth-generation dna sequencing technology. *Genomics, proteomics & bioinformatics* **13**, 4–16 (2015).
5. L Steinbock, A Radenovic, The emergence of nanopores in next-generation sequencing. *Nanotechnology* **26**, 074003 (2015).
6. M Tsutsui, M Taniguchi, K Yokota, T Kawai, Identifying single nucleotides by tunnelling current. *Nat. Nanotechnol.* **5**, 286–290 (2010).
7. M Zwolak, M Di Ventra, Physical approaches to dna sequencing and detection. *Rev. Mod. Phys.* **80**, 141 (2008).
8. M Di Ventra, M Taniguchi, Decoding dna, rna and peptides with quantum tunnelling. *Nat. Nanotechnol.* **11**, 117–126 (2016).
9. P Jing, F Haque, D Shu, C Montemagno, P Guo, One-way traffic of a viral motor channel for double-stranded dna translocation. *Nano Lett.* **10**, 3620–3627 (2010).
10. M Muthukumar, Mechanism of dna transport through pores. *Annu. Rev. Biophys. Biomol. Struct.* **36**, 435–450 (2007).
11. J Chen, A Tsai, SE O'Leary, A Petrov, JD Puglisi, Unraveling the dynamics of ribosome translocation. *Curr. Opin. Struc. Biol.* **22**, 804–814 (2012).
12. E Schleiff, T Becker, Common ground for protein translocation: access control for mitochondria and chloroplasts. *Nat. Rev. Mol. Cell Biol.* **12**, 48–59 (2011).
13. LF Llu, L Perkocha, R Calendar, JC Wang, Knotted dna from bacteriophage capsids. *Proc. Natl. Acad. Sci. USA* **78**, 5498–5502 (1981).
14. DW Sumners, SG Whittington, Knots in self-avoiding walks. *J. Phys. A: Math. Gen.* **21**, 1689–1694 (1988).
15. ML Mansfield, Are there knots in proteins? *Nat. Struct. Mol. Biol.* **1**, 213–214 (1994).
16. WR Taylor, A deeply knotted protein structure and how it might fold. *Nature* **406**, 916–919 (2000).
17. VV Rybenkov, NR Cozzarelli, AV Vologodskii, Probability of dna knotting and the effective diameter of the dna double helix. *Proc. Natl. Acad. Sci. USA* **90**, 5307 (1993).
18. JI Sułkowska, EJ Rawdon, KC Millett, JN Onuchic, A Stasiak, Conservation of complex knotting and slipknotting patterns in proteins. *Proc. Natl. Acad. Sci. USA* **109**, E1715–E1723 (2012).
19. C Micheletti, D Marenduzzo, E Orlandini, Polymers with spatial or topological constraints: Theoretical and computational results. *Phys. Reports* **504**, 1 (2011).
20. SE Jackson, A Suma, C Micheletti, How to fold intricately: using theory and experiments to unravel the properties of knotted proteins. *Curr. Opin. Struc. Biol.* **42**, 6–14 (2017).
21. J Arsuaga, , et al., Knotting probability of dna molecules confined in restricted volumes: Dna knotting in phage capsids. *Proc. Natl. Acad. Sci. USA* **99**, 5373 (2002).
22. J Arsuaga, et al., Dna knots reveal a chiral organization of dna in phage capsids. *Proc. Natl. Acad. Sci. USA* **102**, 9165–9169 (2005).
23. L Huang, DE Makarov, Translocation of a knotted polypeptide through a pore. *J. Chem. Phys.* **129**, 121107–121107 (2008).
24. D Marenduzzo, et al., Dna–dna interactions in bacteriophage capsids are responsible for the observed dna knotting. *Proc. Natl. Acad. Sci. USA* **106**, 22269–22274 (2009).
25. R Matthews, AA Louis, JM Yeomans, Knot-controlled ejection of a polymer from a virus capsid. *Phys. Rev. Lett.* **102**, 088101 (2009).
26. P Virnau, A Mallam, S Jackson, Structures and folding pathways of topologically knotted proteins. *J. Phys. Condens. matter* **23**, 033101 (2011).
27. A Rosa, M Di Ventra, C Micheletti, Topological jamming of spontaneously knotted polyelectrolyte chains driven through a nanopore. *Phys. Rev. Lett.* **109**, 118301 (2012).
28. D Marenduzzo, C Micheletti, E Orlandini, DW Sumners, Topological friction strongly affects viral dna ejection. *Proc. Natl. Acad. Sci. USA* **110**, 20081–20086 (2013).
29. P Szymczak, Translocation of knotted proteins through a pore. *Eur. Phys. J. Special Top.* **223**, 1805–1812 (2014).
30. A Suma, A Rosa, C Micheletti, Pore translocation of knotted polymer chains: How friction depends on knot complexity. *ACS Macro Lett.* **4**, 1420–1424 (2015).
31. V Narsimhan, CB Renner, PS Doyle, Translocation dynamics of knotted polymers under a constant or periodic external field. *Soft matter* **12**, 5041–5049 (2016).
32. FC Rieger, P Virnau, A monte carlo study of knots in long double-stranded dna chains. *PLoS Comput. Biol* **12**, e1005029 (2016).
33. M Wojciechowski, À Gómez-Sicilia, M Carrión-Vázquez, M Cieplak, Unfolding knots by proteasome-like systems: simulations of the behaviour of folded and neurotoxic proteins. *Mol. Biosyst.* **12**, 2700–2712 (2016).
34. C Plesa, et al., Direct observation of dna knots using a solid-state nanopore. *Nat. Nanotechnol.* **11**, 1093–1097 (2016).
35. AY Grosberg, Y Rabin, Metastable tight knots in a wormlike polymer. *Phys. Rev. Lett.* **99**, 217801 (2007).
36. TE Ouldridge, AA Louis, JP Doye, Structural, mechanical, and thermodynamic properties of a coarse-grained dna model. *J. Chem. Phys* **134**, 02B627 (2011).
37. P Šulc, et al., Sequence-dependent thermodynamics of a coarse-grained dna model. *J. Chem. Phys* **137**, 135101 (2012).
38. L Rovigatti, P Šulc, IZ Reguly, F Romano, A comparison between parallelization approaches in molecular dynamics simulations on gpus. *J. Comput. Chem.* **36**, 1–8 (2015).
39. BE Snodin, et al., Introducing improved structural properties and salt dependence into a coarse-grained model of dna. *J. Chem. Phys* **142**, 234901 (2015).
40. SW Kowalczyk, DB Wells, A Aksimentiev, C Dekker, Slowing down dna translocation through a nanopore in lithium chloride. *Nano Lett.* **12**, 1038–1044 (2012).
41. F Farahpour, A Maleknejad, F Varnik, MR Ejtehadi, Chain deformation in translocation phenomena. *Soft Matter* **9**, 2750–2759 (2013).
42. AY Grosberg, Y Rabin, Dna capture into a nanopore: interplay of diffusion and electrohydrodynamics. *J. Chem. Phys* **133**, 10B617 (2010).
43. M Muthukumar, Theory of capture rate in polymer translocation. *J. Chem. Phys* **132**, 05B605 (2010).
44. M Wanunu, W Morrison, Y Rabin, AY Grosberg, A Meller, Electrostatic focusing of unlabelled dna into nanoscale pores using a salt gradient. *Nat. Nanotechnol.* **5**, 160–165 (2010).
45. VV Palyulin, T Ala-Nissila, R Metzler, Polymer translocation: the first two decades and the recent diversification. *Soft Matter* **10**, 9016–9037 (2014).
46. C Micheletti, D Marenduzzo, E Orlandini, DW Sumners, Simulations of knotting in confined circular dna. *Biophys J.* **95**, 3591–3599 (2008).
47. T Ikonen, A Bhattacharya, T Ala-Nissila, W Sung, Unifying model of driven polymer translocation. *Phys. Rev. E* **85**, 051803 (2012).
48. C Plesa, N van Loo, P Ketterer, H Dietz, C Dekker, Velocity of dna during translocation through a solid-state nanopore. *Nano Lett.* **15**, 732–737 (2014).
49. T Sakaue, Nonequilibrium dynamics of polymer translocation and straightening. *Phys. Rev. E* **76**, 021803 (2007).
50. P Rowghanian, AY Grosberg, Force-driven polymer translocation through a nanopore: an old problem revisited. *J. Phys. Chem. B* **115**, 14127–14135 (2011).
51. J Sarabadani, T Ikonen, T Ala-Nissila, Iso-flux tension propagation theory of driven polymer translocation: The role of initial configurations. *J. Chem. Phys* **141**, 214907 (2014).
52. Y Kantor, M Kardar, Anomalous dynamics of forced translocation. *Phys. Rev. E* **69**, 021806 (2004).
53. C Chatelain, Y Kantor, M Kardar, Probability distributions for polymer translocation. *Phys. Rev. E* **78**, 021129 (2008).
54. AY Grosberg, S Nechaev, M Tamm, O Vasilyev, How long does it take to pull an ideal polymer into a small hole? *Phys. Rev. Lett.* **96**, 228105 (2006).
55. C Forrey, M Muthukumar, Langevin dynamics simulations of ds-dna translocation through synthetic nanopores. *J. Chem. Phys.* **127**, 015102 (2007).
56. T Ikonen, A Bhattacharya, T Ala-Nissila, W Sung, Influence of pore friction on the universal aspects of driven polymer translocation. *EPL* **103**, 38001 (2013).
57. S Carson, J Wilson, A Aksimentiev, M Wanunu, Smooth dna transport through a narrowed pore geometry. *Biophys. J.* **107**, 2381–2393 (2014).
58. L Dai, CB Renner, PS Doyle, Metastable tight knots in semiflexible chains. *Macromolecules* **47**, 6135–6140 (2014).
59. PG Dommersnes, Y Kantor, M Kardar, Knots in charged polymers. *Phys. Rev. E* **66**, 031802 (2002).
60. B Marcone, , et al., What is the length of a knot in a polymer? *J. Phys. A: Math. Gen.* **38**, L15 (2005).
61. M Caraglio, C Micheletti, E Orlandini, Stretching response of knotted and unknotted polymer chains. *Phys. Rev. Lett.* **115**, 188301 (2015).
62. S Kirmizialtin, DE Makarov, Simulations of the untying of molecular friction knots between individual polymer strands. *J. Chem. Phys.* **128**, 094901 (2008).
63. V Narsimhan, CB Renner, PS Doyle, Jamming of knots along a tensioned chain. *ACS Macro Lett.* **5**, 123–127 (2016).
64. D Racko, F Benedetti, J Dorier, Y Burnier, A Stasiak, Generation of supercoils in nicked and gapped dna drives dna unknotting and postreplicative decatenation. *Nucleic Acids Res.* **43**, 7229 (2015).
65. L Tubiana, E Orlandini, C Micheletti, Probing the entanglement and locating knots in ring polymers: a comparative study of different arc closure schemes. *Prog. Theor. Phys.* **191**, 192–204 (2011).